

Preclinical efficacy of combinatorial B7-H3 CAR T cells and ONC206 against diffuse intrinsic pontine glioma

Authors

Andrea Timpanaro¹, Edward Z. Song¹, Ryma Toumi¹, Leonel Elena-Sanchez¹, Michael Meechan¹, Caroline Piccand², Kelsey Nemec¹, Anja Kordowski¹, Davina Lau¹, Scott Johnson¹, Lily Winter¹, Ashmitha Rajendran^{1,4}, Rebecca Ronsley^{1,3,5}, Shannon K. Oda^{1,3}, Joshua Gustafson⁵, Jason P. Wendler⁵, Carl Koschmann⁶, Myron Evans^{1,3}, Siobhan Pattwell^{1,3}, Michael C. Jensen⁵, Jessica B. Foster^{7,8}, Matthew D. Dun^{9,10,11}, Matthew C. Biery¹, Nicholas A. Vitanza^{1,3,5}

Affiliations

¹Ben Towne Center for Childhood Cancer and Blood Disorders Research, Seattle Children's Research Institute, Seattle, WA, USA

²Translational Cancer Research, Department for BioMedical Research (DBMR), University of Bern, Switzerland

³Department of Pediatrics, Seattle Children's Hospital, University of Washington, Seattle, WA, USA

⁴Biomedical Informatics and Medical Education, University of Washington School of Medicine, Seattle, WA

⁵Seattle Children's Therapeutics, Seattle, WA, USA

⁶Division of Pediatric Hematology/Oncology, Department of Pediatrics, University of Michigan, Ann Arbor, MI, USA

⁷Division of Oncology, Children's Hospital of Philadelphia, Philadelphia, PA, USA

⁸Department of Pediatrics, University of Pennsylvania Perelman School of Medicine, Philadelphia, PA, USA

⁹Cancer Signalling Research Group, School of Biomedical Sciences and Pharmacy, College of Health, Medicine and Wellbeing, University of Newcastle, Newcastle, New South Wales, Australia

¹⁰Precision Medicine Research Program, Hunter Medical Research Institute, Newcastle, New South Wales, Australia.

¹¹Paediatric Stream, Mark Hughes Foundation Centre for Brain Cancer Research, College of Health, Medicine and Wellbeing, Newcastle, New South Wales, Australia

Key Points:

- B7-H3 CAR T cells are cytotoxic against preclinical DMG models.
- ONC206 causes metabolic apoptosis in preclinical DMG models.
- B7-H3 CAR T cells and ONC206 have combinatorial efficacy against DMG.

Key Words: DIPG, immunotherapy, CAR T cell therapy, B7-H3, ONC206

ABSTRACT

Background. Diffuse intrinsic pontine glioma (DIPG) is a fatal pediatric brain tumor affecting over 300 children annually in the United States. Chimeric antigen receptor (CAR) T cells are a targeted immune effector cell therapy with substantial clinical benefit against hematologic cancers. Against CNS tumors, CAR T cells targeting B7-H3, a protein highly expressed on DIPG, have rapidly advanced from preclinical studies to clinical trials. BrainChild-03 (NCT04185038), a phase 1 trial of repeatedly delivered intracerebroventricular (ICV) B7-H3-targeting CAR T cells (B7-H3 CAR T cells), demonstrated tolerability and potential efficacy for children and young adults with DIPG. However, clinical benefits were not uniformly seen, and multi-agent treatment strategies may be required against such an aggressive disease. Here, we combined B7-H3 CAR T cells with ONC206, an imipridone molecule also under clinical investigation.

Methods. We tested B7-H3 CAR T cells combined with ONC206 across multiple DIPG cell cultures and orthotopic xenograft mouse models.

Results. B7-H3 CAR T cell monotherapy induced robust cytotoxicity while ONC206 treatment resulted in significant mitochondrial dysfunction against DMG/DIPG cells. The combination of low effector-to-target ratios of B7-H3 CAR T cells and IC₅₀ concentrations of ONC206 led to significantly enhanced cytotoxicity *in vitro* ($p < 0.003$) and increased IL-2, IL-29, VEGF-A, and Granzyme B levels. In vivo combinatorial studies of ONC206 and a single ICV dose of B7-H3 CAR T cells significantly extended survival in multiple DIPG xenograft mouse models ($p < 0.05$).

Conclusions. B7-H3 CAR T cells combined with ONC206 is a feasible and efficacious multi-agent approach against multiple DIPG models.

Importance of the study

Diffuse intrinsic pontine glioma (DIPG) is a fatal pediatric brain tumor. While B7-H3 CAR T cells have shown tolerability and potential benefit in early trials, combinatorial regimens may be required for consistent cures against this aggressive disease. This study demonstrates that a preclinical therapeutic regimen of B7-H3 CAR T cells with ONC206, a second-generation imipridone, increases anti-tumor efficacy in vitro and in orthotopic DIPG mouse models. To our knowledge, this is the first study to evaluate ONC206 in combination with CAR T cells. Our findings provide a preclinical roadmap for evaluating small molecules with CAR T cells to interrogate both their combined benefit and the effect of small molecules on T cells themselves. This work offers a biologically-informed, clinically translatable strategy integrating small molecule therapeutics with CAR T cell therapy and support the development of multi-agent immunotherapy trials for children with DIPG and other high-grade brain and spinal cord tumors.

MANUSCRIPT

Introduction

Diffuse intrinsic pontine glioma (DIPG), the most common form of diffuse glioma (DMG), is a fatal pediatric brain tumor most diagnosed in children between the ages of 5 and 10 years¹. The prognosis remains dismal, with a median survival time of less than 12 months from diagnosis. The treatment of DIPG is challenging due to its critical location in the brainstem, where substantial resection is not feasible. These tumors further harbor resistance to conventional therapies underscoring a critical need for novel therapeutic approaches². Recent advances in immunotherapy, particularly chimeric antigen receptor (CAR) T cell therapy, have opened new avenues for cancer treatment. B7-H3, a transmembrane protein involved in regulating T cell response^{3,4} has emerged as a promising therapeutic CAR T cell target on DIPG⁵⁻⁸. This cell surface protein was also found to be upregulated in a range of tumors including atypical teratoid rhabdoid tumors (ATRT)⁹, craniopharyngioma^{10,11}, glioblastoma (GBM)^{12,13}, high-grade glioma (HGG)^{6,14}, medulloblastoma (MB)^{15,16}, meningioma^{17,18}, neuroblastoma (NB)¹⁹, and rhabdomyosarcoma (RMS)^{20,21}.

Seattle Children's first-in-human phase 1 clinical trial (BrainChild-03, NCT04185038) investigated safety and feasibility of B7-H3-targeting CAR T cells (B7-H3 CAR T cells) as locoregional immunotherapy against DIPG, DMG, and recurrent or refractory pediatric central nervous system (CNS) tumors. This trial demonstrated the tolerability of multiple intracerebroventricular (ICV) doses of B7-H3 CAR T cells at up to 100 million cells/dose given to young children in the outpatient setting⁸. While three patients were alive beyond four years from diagnosis, response to treatment was not uniform, suggesting the potential benefit of multi-agent therapy.

To enhance the efficacy of B7-H3 CAR T cells, we have investigated the combination with small molecules to modulate tumor susceptibility to immunotherapy. Among these, we tested imipridones, pro-apoptotic compounds characterized by a tricyclic core structure able to target dopamine receptor D2 (DRD2) and induce an anti-proliferative effect on cancer cells by modulating the AKT and ERK signaling pathways²². Novel studies have proven the capacity of imipridones to bind to the caseinolytic protease proteolytic subunit (ClpP) and activate the integrated stress response (ISR) cascade^{23,24}. One class member, ONC201, has been evaluated in various tumor types including, brain cancers and demonstrated the ability to cross the blood-brain barrier^{25,26}. ONC206, an analog of ONC201 with a greater binding affinity and selectivity²⁷,

follows the same mechanism of action by inducing apoptosis and stress-related signaling pathways in multiple models and may be more cytotoxic against DIPG²⁸.

Here, we investigate the combinatorial potential of B7-H3 CAR T cells with ONC206 to enhance treatment efficacy against DIPG. Harnessing the tumor-targeting specificity of B7-H3 CAR T cells with the pro-apoptotic and stress-inducing properties of ONC206; this approach aims to increase tumor susceptibility to immunotherapy while maintaining treatment tolerability. Ultimately, this study explores the potential to combine targeted cellular therapy with small molecules to improve treatments against DIPG.

Methods

All vendors and corresponding catalog numbers for the used materials are reported in Table 1.

Human specimen and patient-derived cell cultures. Human cell cultures were established with informed consent under institutional review board approval from Seattle Children's Hospital (#14449). Biopsy specimens PBT-22FH, PBT-24FH, PBT-27FH, and PBT-29FH were acquired at diagnosis. The tumor tissues were procured at Seattle Children's Hospital, and subsequent cell cultures were developed at Fred Hutchinson Cancer Research Center (FHCRC). SU-DIPG-XIII cell line was generously provided by Dr. Michelle Monje. These cell lines were cultured in NeuroCult NS-A Basal Medium supplemented with NS-A Proliferation Supplement (Stemcell Technologies), 40 ng/mL epidermal growth factor, and 40 ng/mL fibroblast growth factor (PeproTech), along with 2 mM GlutaMax (Gibco). Lenti-X 293T cells, used for CAR lentivirus production, were kindly provided by Prof. Michele Bernasconi and cultured in DMEM medium (Gibco) supplemented with 10% of fetal bovine serum (FBS) (Thermofisher). All cell culture models were validated with periodic DNA fingerprinting prior to experimentation.

Lentivirus production. Lentiviruses (LVs) were generated via transfection of Lenti-X 293T cells, kindly provided by Prof. Bernasconi (University of Bern). 5×10^6 293T cells were seeded onto P10 plates, pre-coated with collagen type I rat tail, and cultured overnight in DMEM medium supplemented with 10% fetal bovine serum and 1x GlutaMax. The day after, 293T cells were co-transfected via calcium phosphate method with 10 µg of psPAX2, 4 µg of pVSV-G, and 10 µg of lentiviral B7-H3 CAR plasmid, as previously described⁵¹. Lentiviruses-containing supernatants

were harvested 48 h post-transfection, filtered with 0.45 µm filters, and concentrated via overnight centrifugation at 4'000xg at 4 °C. Lentiviruses were aliquoted and stored at -80 °C until use.

CAR T cell manufacturing. T cells were isolated from peripheral blood mononuclear cells (PBMCs) of healthy donors (Bloodworks Northwest) by negative selection using the EasySep™ human T cell isolation kit. T cells were then stimulated with anti-CD3/CD28 Dynabeads (Gibco, #40203D) at 1×10^6 cells/mL for 36 h and transduced at a multiplicity of infection of 5 with LVs titrated as previously described⁵¹. Transduced cells were counted every other day and maintained at a density of 0.8×10^6 cells/mL in RPMI-1640 medium supplemented with 10% fetal bovine serum, 1x GlutaMax, 5 ng/mL recombinant human IL-7, and 0.5 ng/mL recombinant human IL-15. After expansion, cells were cryopreserved in CryoStor® CS10 in liquid nitrogen until use.

Bioluminescence survival assays. Bioluminescence killing assays were conducted by seeding at day 0 5'000 iRFP720⁺ firefly luciferase-positive (fLuc⁺) tumor cells onto a bioluminescence-compatible 96-well plate in 150 µl of NeuroCult medium (Stemcell). 50 µl of ONC206 at the final concentration of 150-300nM and/or 50 µl of B7-H3 CAR T cells at various effector-to-target (E:T) ratios of 1:10, 1:4, 1:2, 1:1, 2:1, and 5:1 were added to the respective wells at day 1. Untransduced mock T cells were used as negative controls. The other controls included 50 µl of medium replacing CAR T cells or ONC206. On the day of measurement, D-Luciferin was diluted in NeuroCult medium at the concentration of 30 µg/ml and administered to the wells. After 10-minute incubation at RT, bioluminescence intensity was quantified using a SpectraMax® iD3 Multi-Mode Microplate Reader (Danaher). Data from the assays were processed using Microsoft Excel and GraphPad Prism 9 for analysis.

Live-imaging cytotoxicity assays. Two or seven-day-long cell viability assays were performed with live-imaging Incucyte technology to monitor tumor cell expansion and killing capacity of B7-H3 CAR T cells. 5'000 firefly luciferase⁺ (fLuc⁺) iRFP720⁺ tumor cells were plated at day 0 onto a black/clear bottom 96-well plate in 150 µl of NeuroCult medium. 50 µl of ONC206, at the final concentrations of 150-300nM, and/or 50 µl of B7-H3 CAR T cells at the various Effector-to-Target (E:T) ratios of 1:10, 1:4, 1:2, 1:1, and 5:1, were added to the respective wells at day 1. The respective control conditions included 50 µl of medium replacing CAR T cells and/or ONC206. Images were acquired every 4h using the Incucyte S3 device (Sartorius). Phase-contrast images were normalized to their respective baseline images taken at day 0. The results were processed with Incucyte 2022B Rev2 and Graphpad Prism 10 software.

Enzyme-linked immunosorbent assays. 50'000 PBT-22FH, PBT-24FH, PBT-27FH, PBT-29FH, and SU-DIPG-XIII cells were plated onto a 24-well plate and co-cultured with 250'000 B7-H3 CAR

T cells (E:T ratio of 5:1) in 1ml of NeuroCult medium (Stemcell). After 24h, the supernatant was collected in 1.5ml tubes and stored at -80 °C until use. To assess the amount of human IL-2, TNF- α , and IFN- γ released by B7-H3 CAR T cells, ELISAs were performed following the manufacturer's instructions. The results were analyzed with Microsoft Excel, whereas the figures were generated using GraphPad Prism 9.

Flow Cytometry. Expression of surface targets was determined using the primary antibodies listed in Table 1. T cell phenotyping to determine the amount of naïve, central memory, and effector T cells included the expression of the following markers: CD62L, CD3, CD4, CD8, CD45RA. The expression of LAG-3, PD-1, and TIM-3 established exhaustion of CAR T cells before and after killing assays. Briefly, samples were washed twice in flow buffer (PBS supplemented with 2% BSA) and incubated at RT for 30 min with the corresponding primary antibodies at the dilution of 1:100. After washing cells twice, fluorescence was measured at the Cytoflex (Beckman). Flow analysis included a gate according to forward scatter/side scatter profiles and a gate on single cells. T cells were selected based on CD3 expression. Transduction efficiency was evaluated after 48 hours on EGFRt expression compared to untransduced T cells (Mock). FlowJo software was used to analyze flow cytometry data.

Seahorse Assay. Oxygen consumption rate (OCR), basal respiration, non-mitochondrial respiration, and extracellular acidification rate (ECAR) were respiratory parameters measured using Seahorse XFe96 Analyzer and Cell Mito Stress Test Kit (Agilent). PBT-22FH, PBT-24FH, PBT-27FH, PBT-29FH, and SU-DIPG-XIII cells were treated with ONC206 at the different concentration of 150, 200, 250, and 300 nM. DMSO-treated cells were used as controls. After 48 hours, DIPG cells were washed and equilibrated to un-buffered medium for 1h at 37°C in a CO₂-free incubator and transferred to the XFe96 analyzer. Reduction in mitochondrial respiration was assessed with sequential administration of 2 μ M oligomycin, 2 μ M carbonyl cyanide p-trifluoromethoxyphenylhydrazone (FCCP), and 0.5 μ M Rotenone/ Antimycin A (AA). The experiments were performed following the manufacturer's instructions, whereas the data were analyzed with Agilent Seahorse Wave Desktop software.

Multiplex immunoassay. To evaluate cytokine release, 100'000 PBT-27FH and PBT-29FH cells were co-cultured with an equal number of CAR T cells in 24-well plates in the presence of ONC206 (250 nM) for 5 days in complete NeuroCult medium. Following incubation, supernatants were collected and analyzed using the human cytokine/chemokine 96-plex discovery assay® (HD96) (Eve Technologies, Calgary, AB, Canada). Cytokine concentrations were quantified and normalized as appropriate for subsequent analysis. All statistical analyses for the cytokine data

were performed in R using the lme4 and emmeans packages. A single linear mixed-effects model was fitted, treating log2-transformed cytokine values as the response variable and including cell line, treatment, and cytokine as fixed effects; donor was included as a random intercept. Linear contrasts (e.g., “ONC206&CAR T vs. CAR T” and “ONC206 vs. PBS”) were calculated to assess differential expression in selected comparisons, with all p-values corrected using the false discovery rate.

RNA sequencing. To perform RNA sequencing, 100,000 DIPG cells were co-incubated in 24-well plates with 100,000 CAR T cells in the presence of ONC206 (250 nM) for 5 days in complete NeuroCult medium. RNA was purified using RNeasy Plus Mini Kit (Qiagen) following the manufacturer’s instructions. RNA samples were sent to Novogene for sequencing. All pre-processing steps were run using Terminal. FastQ files were downloaded from Novogene and processed using FastP^{52,53} to filter reads and trim adaptors, followed by FastQC to evaluate quality. Reads were pseudoaligned to the human GRCh38 cDNA transcriptome (Ensembl release 113)⁵⁴ using Kallisto (version 0.51.1)⁵⁵ and run through MultiQC⁵⁶ to assess post-mapping quality. All post-processing steps were run using RStudio (version 2024.12.0+467; R Core Team, 2022). Transcripts were summarized to the gene level via tximport (version 1.34.0)⁵⁷ and abundance counts were calculated via TPM, followed by normalization using TMM via edgeR (version 4.4.2)⁵⁸⁻⁶⁰. PCA plots were made using the “prcomp” function. Differential gene expression analysis was performed using linear modeling via limma (version 3.62.2)⁶¹ and differentially expressed genes were called by applying cutoffs for FDR (0.05), counts per million (CPM) in at least one of the comparators (+1), and Log₂(FC) (+/- 2). Statistical overrepresentation tests and related GO Terms were calculated using the Panther Classification System (Version 19.0). Respective lists of upregulated DEGs were manually imported into the Gene List Analysis tab, selected for homo sapiens, and run through the statistical overrepresentation test option using the “GO biological process complete” option. Tests were run using the Fisher’s Exact option with an FDR threshold of 0.05. Related figures were created using GraphPad Prism (version 10.4.1).

Surgical procedure and in vivo experimentation. 8-week-old immunodeficient NOD.Cg-Prkdcscid Il2rgtm1Wjl/SzJ (NSG) female mice were purchased from Jackson Lab and housed at the Animal Facility of the Seattle Children’s Research Institute, under pathogen-free conditions. The experiments were approved by the Institutional Animal Care and Use Committee (IACUC) and conducted following the protocol #ACUC00669. Intracranial xenografts were established injecting 50’000 SU-DIPG-XIII cells, expressing a bicistronic cassette including mCherry and Firefly Luciferase (fLuc⁺), at 0.8 r lateral, 1.5 mm posterior, and 2.5 mm deep, relative to lambda.

Each cohort contained at least seven mice for adequate power. Only mice with confirmed tumor engraftment were maintained in the study and included in all analyses. 1 million Mock/CAR T cells were intracerebroventricularly (ICV) injected, whereas ONC206 was orally administered twice a week at the concentration of 50 mg/kg. For PBT-29FH study, little chunk tumors were chopped and injected using the same coordinates, whereas 250'000 Mock/CAR T cells were intracerebroventricularly (ICV) injected. Tumor growth was weekly monitored via optical imaging (In Vivo Imaging System), and mouse weights were measured twice a week. Symptomatic mice were euthanized, and tumors were post-mortem resected for IHC analysis.

Statistical analyses. Statistical analyses were performed using GraphPad prism 9.0 (GraphPad Software, Inc., La Jolla, CA, USA). Dose-response curves were generated using nonlinear regression [log (inhibitor) vs. response - Variable slope (four parameters)]. Cell proliferation was analyzed using a two-way ANOVA (Sidak's multiple comparison). Seahorse data were analyzed using one-way ANOVA (Tukey's multiple comparison). For mice survival, Kaplan–Meier method (Kaplan–Meier survival fractions) was used to calculate the Log-rank (Mantel–Cox) and generate p-values. The statistical significance between experimental and control triplicate groups was analyzed incorporating a Dunnett's multiple comparison test following a two-way ANOVA to examine main effects and interactions between variables. The levels of significance will be indicated as follows: $p > 0.05$ (ns), $p \leq 0.05$ (*), $p \leq 0.01$ (**), $p \leq 0.001$ (***), $p \leq 0.0001$ (****).

Illustrations. Schemas and illustrations were generated with BioRender.com.

Results

On-target effector function of B7-H3 CAR T cells against DMG/DIPG models with high target expression

We first assessed the expression of B7-H3 on treatment-naïve, patient-derived DMG/DIPG models (PBT-22FH, PBT-24FH, PBT-27FH, PBT-29FH^{29,30}) and an autopsy-derived model (SU-DIPG-XIII). Consistent with several other reports^{5,6,31,32}, the quantification of surface copy numbers revealed a high density of B7-H3 at the protein level, with a minimum density of 30,000 molecules per cell and over 200,000 molecules on PBT-24FH (Figure 1A).

To assess B7-H3 CAR T cell efficacy, co-incubation experiments were performed at various effector-to-target (E:T) ratios (1:10, 1:4, 1:2, 1:1, 2:1, and 5:1) and cytotoxicity was evaluated after 48 hours. Data from three independent CAR T cell donors confirmed high killing ability, with >50%

tumor cell lysis observed at the E:T ratio of 1:1 (Figure 1B). Notably, PBT-24FH - a hypermutant DIPG³³ - exhibited greater sensitivity, with a 40% reduction in survival at the lowest E:T ratio of 1:10 (Figure 1B, red). To investigate long-term efficacy at low CAR T cell doses and to optimize conditions for evaluating potential synergy with ONC206, live-imaging experiments were performed considering multiple time-points (Figure 1C). Consistent with previous findings, an E:T ratio of 1:1 confirmed a cytostatic-like effect in most models, while PBT-24FH cells were eradicated more rapidly. Of note, higher doses of CAR T cells resulted in excessive tumor cell lysis, limiting the ability to distinguish potential synergistic effects of combination therapies. Therefore, E:T ratios of 1:10, 1:4, and 1:2 were selected for subsequent combinatorial studies with ONC206.

The efficacy of B7-H3 CAR T cells was further characterized by quantifying cytokine release, including IL-2, TNF- α , and IFN- γ . Supernatants were collected after 24 hours of co-incubation of CAR T cells with DIPG models. The results demonstrated that B7-H3 CAR T cells produced significantly elevated levels of IL-2, IFN- γ , and TNF- α compared to mock T cells, with the most robust cytokine response observed against PBT-24FH cells (~1750 pg/ml IL-2, ~1000 pg/ml IFN- γ , and ~700 pg/ml TNF- α ; Figure 1D).

These findings not only validated the cytotoxic activity of B7-H3 CAR T cells in our DIPG models but also guided the selection of optimal E:T ratios for subsequent studies investigating the combinatorial potential with ONC206.

ONC206 demonstrates limited effects on CAR T cell proliferation

To explore promising therapeutic options to combine with B7-H3 CAR T cells, we selected several candidate drugs based on previously reported efficacy in preclinical and clinical DIPG models. Marizomib has shown promise as a proteasome inhibitor capable of crossing the blood-brain barrier, warranting its inclusion in ongoing studies for DIPG treatment^{34,35}. ONC206, an imipridone derivative of ONC201, has shown significant potency and improved efficacy against DIPG cells both *in vitro* and *in vivo*, making it a promising therapeutic candidate currently under clinical investigation^{27,36}. Paxalisib, targeting the PI3K/mTOR pathway, has shown encouraging preclinical results and is being evaluated in clinical trials specifically for DMG/DIPG³⁷⁻³⁹. Zotiraciclib, a CDK9 inhibitor, exhibits strong anti-glioma effects in preclinical studies, suggesting its potential applicability in treating DIPG⁴⁰. Additionally, everolimus, an mTOR inhibitor, and conventional chemotherapeutic agents, such as carboplatin, etoposide, and vincristine, were tested against pediatric CNS tumors.

To assess baseline drug sensitivity, IC₅₀ values were determined after 120 hours of treatment using Cell Titer-Glo assays in two representative DMG models: the H3.1-mutant PBT-27FH and the H3.3-mutant PBT-29FH (Figure 2A-C). We then tested the drugs for potential compatibility with B7-H3 CAR T cell therapy. CAR T cells were co-cultured with tumor cells at a 5:1 E:T ratio for 24 hours to allow for antigen-mediated activation. Subsequently, each drug was added at its respective IC₅₀ concentration, and CAR T cell survival and expansion were monitored for five days. The experimental workflow allowed for CAR T cell activation through antigen recognition before drug exposure, isolating the effect of the compounds on CAR T cell viability.

As shown in the viability curves (pre-co-incubation with PBT-27FH - Figure 2D - or PBT-29FH cells - Figure 2E) and fold-change expansion compared to B7-H3 CAR T cell treated with vehicle (Figure 2F-G), ONC206 stood out for its dual profile: anti-tumor cytotoxicity and minimal adverse effects on CAR T cell expansion. In contrast, several other compounds either impaired CAR T cell proliferation or lacked comparable tumoricidal activity. Paxalisib was not further explored here due to a parallel project⁴¹, whereas marizomib and carboplatin, despite lack of toxicity on CAR T cells were discarded due to their low potency against DIPG cells. These findings led us to prioritize ONC206 for downstream combination strategies with B7-H3 CAR T cells.

ONC206 demonstrates robust induced apoptosis across multiple DIPG models

ONC206, a member of the imipridone family, has emerged as a potential anti-cancer agent due to its abilities to specifically recognize ClpP and DRD2 and induce apoptosis through pathways involving mitochondrial dysfunction and stress response signaling^{27,28,42,43}. To evaluate the cytotoxicity of ONC206, we performed dose titration experiments on five different DIPG/DMG models - PBT-22FH, PBT-24FH, PBT-27FH, PBT-29FH, and SU-DIPG-XIII - identifying an IC₅₀ range of 217 - 298 nM after 120 hours (Figure 3A), leading to the selection of the averaged inhibitory dose of 250 nM for further studies.

Early apoptosis was evaluated using annexin-V staining and flow cytometry after 48 hours of treatment. For this experiment, a higher concentration of 500 nM was included to fully assess the apoptotic trend. As expected, a moderate dose-dependent increase in annexin-V levels was observed (Figure 3B), with higher responses at 500 nM, particularly in PBT-24FH, PBT-27FH, and PBT-29FH. In contrast, SU-DIPG-XIII showed minimal annexin-V expression (0.5% at 250 nM; 0.2% at 500 nM), indicating potential intrinsic resistance or activation of protective pathways in this model - similar ONC201 results were already observed in SU-DIPG-XIII model, revealing mechanisms linked to upregulated redox PI3K signaling⁴⁴.

Live-cell imaging over seven days using a larger range of ONC206 concentrations (0.01 μ M to 100 μ M) and detecting caspase-3/7 expression via fluorescent dye confirmed a concentration-dependent apoptotic response (Figure 3C), where concentrations ≥ 1 μ M induced rapid apoptosis in most models, while lower concentrations (< 0.03 μ M) had minimal effects. Remarkably, near- IC_{50} levels (0.32 μ M) exhibited a distinct peak in caspase-3/7 activity at approximately 120 hours in most models, establishing this as optimal time-point for further experiments. As previously observed, SU-DIPG-XIII showed a delayed response with apoptosis peaking at 168 hours when ONC206 was used at 0.32 μ M, supporting the notion of greater apoptosis-resistance. The inclusion of vehicle-treated controls further validated the specificity of the apoptotic response following negligible activation of caspase-3/7.

ONC206 caused significant cytotoxicity across all the cultures, with complete cell death observed within seven days at doses ≥ 0.32 μ M (Figure 3D) highlighting effective cytotoxicity across the investigated DIPG models, with implications for combining it with B7-H3 CAR T cells to optimize therapeutic outcomes.

To further characterize the pro-apoptotic effects of ONC206 in DIPG, we performed RNA sequencing following a 120-hour co-culture with CAR T cells and ONC206 treatment (250 nM) against PBT-27FH and PBT-29FH. Sequencing yielded high-quality transcriptomes with Phred scores > 35 from two biological replicates per condition (Supplemental Fig.1A). Read alignment and mapping statistics confirmed efficient annotation to the human transcriptome (Supplemental Fig.1A). Principal component analysis (PCA) revealed distinct clustering between ONC206 and vehicle-treated samples, demonstrating strong treatment-driven transcriptional divergence in both models (Supplemental Fig.1B).

Differential expression analysis identified 6,953 genes significantly altered in PBT-27FH and 7,404 in PBT-29FH (adjusted p-value < 0.05). To refine our analysis to biologically meaningful transcripts, we applied stringent thresholds ($\log_2FC > 2$ and CPM > 1), yielding 381 and 390 significantly upregulated genes in PBT-27FH and PBT-29FH, respectively (Supplemental Fig.1C). Comparison of these gene sets revealed a shared core of 140 commonly upregulated genes, with each model also exhibiting distinct transcriptomic signatures (Supplemental Fig.1D).

Gene ontology (GO) enrichment analysis of upregulated genes highlighted a strong overrepresentation of biological processes related to programmed cell death (GO:0043067),

including subclasses such as positive regulation of apoptotic process (GO:0043065) and intrinsic apoptotic signaling pathway in response to endoplasmic reticulum stress (GO:0070059) (Supplemental Fig.1E). Building on our caspase-3/7 activation data, we focused specifically on the subset of pro-apoptotic genes within GO:0043065. A total of 37 pro-apoptotic genes were significantly upregulated in at least one of the two models upon ONC206 treatment, including key regulators such as ATF3, BBC3, BMF, DDIT3, FOSL1, and TNFRSF10B (DR5), supporting a consistent transcriptional shift toward apoptosis (Supplemental Fig.1F).

ONC206 selectively disrupts tumor cell metabolism while preserving CAR T cell bioenergetics

Based on preliminary cytotoxicity results, we examined the effects of ONC206 on the metabolism of DIPG models at relevant concentrations near the IC₅₀ (150 nM, 200 nM, 250 nM, and 300 nM). Given its known anti-tumor activity, we aimed to assess its impact on mitochondrial respiration and overall bioenergetic profiles, while also evaluating potential impairments in B7-H3 CAR T cell metabolism to determine its suitability for combination therapies. PBT-22FH, PBT-24FH, PBT-27FH, PBT-29FH, SU-DIPG-XIII, and CAR T cells were treated for 48 hours with ONC206, while control cells were cultured with the vehicle. After incubation, cellular metabolism was measured by using Seahorse technology, sequentially adding oligomycin, FCCP, and rotenone/antimycin A compounds to test mitochondrial stress.

Targeting cells at a low ONC206 dose (150 nM) demonstrated a selective impact on the metabolic profiles, highlighting a higher potential in inducing cell stress (Figure 4). Notably, a drastic dose-metabolic stress response was observed in all the DIPG lines tested in a dose-dependent manner (Figure S2). By contrast, CAR T cell metabolism was minimally impaired at IC₅₀ doses (Figure 4A, bottom-right). In general, ONC206 treatment at 250 nM led to a complete collapse of mitochondrial respiration, as evidenced by the oxygen consumption rate (OCR) profiles (Figure 4A, red lines). Maximal respiration, as measured after FCCP treatment, was abolished, with tumor cells showing a lack of spare respiratory capacity (SRC) (Figure S2). Fold-change quantification across the DIPG cultures showed that ONC206 reduced basal respiration by over 90% compared to vehicles (Figure 4B, $p < 0.0001$), indicating severe mitochondrial dysfunction. ATP-linked respiration and non-mitochondrial respiration were significantly reduced in most DIPG tumor cells ($p < 0.05$ to $p < 0.001$), except for PBT-24FH, which exhibited partial resistance (Figure S2). Additional respiratory parameters evaluated exhibited complete loss of SRC under the same conditions. Furthermore, bioenergetic profiles indicate that ONC206 effectively disrupts the

respiratory capacity of DIPG cells, driving PBT-22FH, PBT-24FH, PBT-27FH, and PBT-29FH into a quiescent state, while shifting SU-DIPG-XIII toward a glycolytic phenotype (Figure 4C & Figure S2, right panels, for the other concentrations).

On the other hand, CAR T cells displayed a different response to ONC206, underscoring their resilience to metabolic stress (Figure 4A, bottom-right panel). Despite a modest reduction in basal respiration ($p < 0.05$), CAR T cells retained over 70% of their OCR under ONC206 treatment, reflecting preserved mitochondrial functionality (Figure 4B, lateral charts). ATP-linked respiration remained largely intact, with a negligible reduction compared to controls. Importantly, maximal respiration was maintained, with CAR T cells retaining their SRC under treatment conditions ($p < 0.05$) (Figure S2X), whereas non-mitochondrial respiration decreased remaining functionally adequate ($p < 0.05$) (Figure S2U). Notably, bioenergetic phenotype analyses underscored that CAR T cells preserved an energetic phenotype among all the experimental conditions with a well-preserved balance of OCR and extracellular acidification rate (ECAR) even at 300 nM (Figure S2Y). This ability to maintain metabolic flexibility and function despite ONC206 treatment highlights the remarkable resilience of CAR T cells to mitochondrial stress.

Increased cytotoxicity of CAR T cell-mediated killing in combination with ONC206

Combinatorial experiments of ONC206 IC_{50} doses and low E:T ratios of B7-H3 CAR T cells were performed on PBT-22FH, PBT-24FH, PBT-27FH, PBT-29FH, and SU-DIPG-XIII to evaluate possible combinatorial benefits. DIPG cells were treated for 120 hours under optimal conditions as previously described for each cell line: Mock T cells (control), ONC206 (IC_{50} -close concentrations), CAR T cells (E:T ratios in the range of 1:10 - 1:4), and combination. Killing capacity was evaluated via Incucyte experiments and luciferase assays.

Seven-day live-imaging experiments revealed a regulated combinatorial killing effect across the entire panel of models (Figure 5A). Single-agent treatments with CAR T cells (orange) and ONC206 (blue) primarily exhibited a cytostatic-like effect compared to the mock group (red). Notably, the impact of the combinatorial treatment (green) became increasingly pronounced over time, leading to statistically significant reduction in tumor cells at later time points, with greater tumor elimination by day 7 in PBT-22FH, PBT-27FH, and PBT-29FH models. Luciferase assays were further performed to measure tumor cell survival after 120 hours and corroborate these results. D-Luciferin was added at the concentration of 10 μ g/mL into the wells, and tumor cell viability was normalized to the vehicle controls. Single treatments showed an efficacy of around

50% in each cell line, while combinatorial groups (green) revealed significantly superior killing across the DIPG culture panel (Figure 5B). These results, confirmed among three different CAR T cell donors, support an improved combinatorial effect mediated by ONC206, which is potentially able to sensitize tumor cell to immune-mediated cytotoxicity, offering the rationale for further preclinical studies.

Functional profile of B7-H3 CAR T cells preserved at low doses of ONC206

To evaluate whether ONC206 IC₅₀ dose influences CAR T cell effector functions, we analyzed T cell phenotypes by assessing the ratios of central memory (T_{CM}), naïve-like (T_N), effector (T_E), and effector memory (T_{EM}) T cells across three different donors. B7-H3 CAR T cells were co-incubated with the representative models PBT-27FH and PBT-29FH at the E:T ratio of 5:1, either in the presence or absence of ONC206 (250 nM). After 5 days, CAR T cells were collected and analyzed by flow cytometry. CAR T cells were then gated for CD3 expression, and T cell subtypes were determined based on CD62L and CD45RA expression. Upon antigen stimulation by either tumor cell model, the proportions of T_{CM} (CD62L⁺/CD45RA⁻), T_E (CD62L⁻/CD45RA⁺), and T_{EM} (CD62L⁻/CD45RA⁻) populations remained consistent (Figure 5C), despite visible variability among donors. Similarly, the CD4/CD8 ratio in the combination groups was unchanged, compared to the respective controls (Figure 5D).

Next, we evaluated the expression of the markers LAG-3, TIM-3, and PD-1 to determine whether ONC206 affects CAR T cell exhaustion. Consistent with the previous results, no differences were observed in the percentage of CAR T cells expressing these markers between the controls and combination groups (Figure 5E) indicating that low doses of ONC206 do not significantly alter CAR T cell phenotypic composition, or CD4/CD8 ratios, nor do they cause CAR T cell exhaustion under these conditions.

ONC206 IC₅₀ dose does not impair cytokine release in activated CAR T cells

To assess the impact of ONC206 on cytokine secretion by B7-H3 CAR T cells, we conducted a comprehensive 96-plex immunoassay, co-culturing CAR T cells with PBT-27FH or PBT-29FH cells at an effector-to-target (E:T) ratio of 1:1 in the presence or absence of ONC206 (250 nM). Following five days of co-culture, supernatants were collected, and cytokine concentrations were quantified and normalized to vehicle-treated controls.

Linear contrast analyses from three independent T cell donors (e.g., fold change comparisons referred to as “ONC206 & CAR T vs. CAR T” and “ONC206 vs. PBS”) revealed that ONC206 does not globally suppress cytokine release by CAR T cells (Figure 5). Regardless of the DIPG model employed to stimulate CAR T cell activation, exposure to ONC206 resulted in a reduction of specific cytokines, including TRAIL, Granzyme A, IL-5, and perforin, compared to controls (Figure 5F, red dots). This effect however was counterbalanced by the significant upregulation of key cytokines such as IL-2, IL-29, IP-10, and VEGF-A (Figure 4F, green dots). Importantly, cytokines typically associated with CAR T cell characterization, including IL-3, IL-6, IL-8, TNF- α , IFN- γ , and Granzyme B, remained consistently sustained even after five days of ONC206 treatment, predominantly around a log2 value of 10, as visualized in the quantitative bubble heatmap (Figure 5G, white circles).

These findings demonstrate that ONC206 at 250 nM preserves CAR T cell cytokine secretion while selectively modulating specific pathways, thereby maintaining overall immune functionality. The sustained production of key cytokines, together with the targeted enhancement of others, supports its profile as a well-tolerated agent that maintains CAR T cell function and therapeutic potential. These results further support the rationale for combining ONC206 with B7-H3 CAR T cells, as its modulatory effects on T cells are likely minimal.

Combination therapy with ONC206 and B7-H3 CAR T cells improves survival and maintains tolerability in orthotopic DIPG mouse models

After demonstrating that low doses of ONC206 significantly increased the killing capacity of B7-H3 CAR T cells *in vitro* without impairing T cell phenotype, exhaustion, and release of functional cytokines, we tested the proposed combinatorial approach in two distinct DIPG mouse models: SU-DIPG-XIII and PBT-29FH. For the SU-DIPG-XIII model, 5×10^4 firefly luciferase-expressing tumor cells were stereotactically injected into NSG mice on day 0 (Figure 6A). Following tumor engraftment and normalization, mice were stratified into four experimental cohorts: a) Mock T cells + vehicle (control); b) Mock T cells + ONC206 (ONC206 monotherapy); c) B7-H3 CAR T cells + vehicle (CAR T monotherapy); and d) B7-H3 CAR T cells + ONC206 (combination therapy). ONC206 administration began on day 3, with a dosing regimen of 50 mg/kg, once daily, twice weekly, maintained until the experiment conclusion. At day 7, 1×10^6 Mock T cells or CAR T cells were ICV delivered. Mice were monitored daily for potential treatment-related side effects, while body weight was recorded weekly. Animals were euthanized upon reaching endpoint criteria, including severe neurological symptoms or >20% body weight loss. The results demonstrated

that ONC206 at 50 mg/kg was well tolerated, with no observed side effects, confirming its suitability for *in vivo* administration. However, ONC206 monotherapy failed to show efficacy in the SU-DIPG-XIII model, as survival was comparable to the control group (Figure 6B). In fact, both the control and ONC206 monotherapy cohorts reached endpoint within 12 days post-T cell injection, with median survival times of 15 and 14 days, respectively. In contrast, the CAR T monotherapy group exhibited a substantial benefit, extending the survival of 2 out of 12 mice up to day 40, with a median survival of 25 days (Figure 6B-D). Notably, the combination therapy significantly outperformed both monotherapy groups ($p < 0.05$), demonstrating a clear advantage in delaying tumor progression as early as day 19. Remarkably, 6 out of 12 mice in the combination group survived beyond day 35 (median survival), and three mice achieved long-term survival, with one reaching up to 101 days (Figures 6B-D). Weight progression data further support the tolerability of the combination treatment, with weight loss occurring only at advanced stages of disease when tumor burden was high (Figure 6D).

For the PBT-29FH model, murine tumor tissues were mechanically dissociated from mouse donors, and small fragments were uniformly implanted into NSG mice on day 0. Unlike the SU-DIPG-XIII model, bioluminescence imaging for PBT-29FH was not feasible, as the implanted tumor fragments lacked a luciferase reporter. Consequently, tumor progression was assessed solely based on mouse survival and weight monitoring. As in the SU-DIPG-XIII model, four experimental cohorts were established, maintaining the same treatment conditions. ONC206 was administered at 50 mg/kg, once daily, twice weekly, whereas 0.25×10^6 mock T cells or B7-H3 CAR T cells were ICV delivered at day 10 (Figure 6F). The Kaplan-Meier survival analysis (Figure 6G) demonstrated a significant survival benefit in the combination therapy group (green line) compared to the mice receiving control treatment (red) or ONC206 monotherapy (blue), the latter of which exhibited the shortest survival, indicating a limited therapeutic efficacy of ONC206 alone in this aggressive model. While B7-H3 CAR T cell monotherapy (orange) extended survival relative to controls, the combination therapy resulted in noticeable improvement, with survival extended until day 85. No toxicity was observed in the combination group, and mouse weight loss was related to tumor (Figure 6G, 6H). Together, the absence of neurological side effects and longer survival in the combination cohort during the whole treatment indicate that ONC206 at 50 mg/kg is well tolerated and does not contribute to significant adverse effects. Collectively, these results highlight that ONC206 may sensitize tumor cells and enhance B7-H3 CAR T cell-mediated tumor control, leading to significant survival benefit.

Discussion

B7-H3 CAR T cell therapy has emerged as a promising strategy for treating DIPG, offering tumor selectivity, therapeutic tolerability, and potential clinical activity^{7,8}. However, obstacles including tumor heterogeneity, a hostile tumor immune microenvironment, low CAR T cell persistence, and the need to target a diffusely invading disease often hamper effective treatment. Therefore, here we attempted to combine B7-H3 CAR T cells with other agents undergoing clinical advancement for improved efficacy.

Here, we confirmed that ONC206 robustly induces apoptosis and metabolic collapse in multiple DIPG models, while preserving the metabolic fitness, phenotype, and effector functions of B7-H3 CAR T cells. Seahorse analyses confirmed that, even at IC₅₀ concentrations (150 - 300 nM), ONC206 selectively impairs tumor cell oxidative metabolism while sparing CAR T cell basal and maximal respiratory capacity. Furthermore, IC₅₀-doses of ONC206 did not significantly alter T cell subset distribution, exhaustion marker expression, or CD4/CD8 ratios, even after prolonged co-culture. Cytokine profiling revealed preserved - or even enhanced - secretion of key effector molecules such as IL-2, VEGF-A, IL-29, IP10, IFN- γ , Granzyme B, and TNF- α by CAR T cells in the presence of ONC206, supporting the notion that IC₅₀-doses of this compound do not compromise T cell functionality.

Critically, combination therapy with ONC206 and B7-H3 CAR T cells led to significantly improved tumor cell elimination and increased killing efficacy *in vitro* across multiple DIPG cultures via both luciferase assays and live-imaging experiments. Beyond *in vitro* analyses, the combinatorial efficacy was further supported *in vivo*, in which mice treated with low doses of B7-H3 CAR T cells and ONC206 exhibited markedly improved tumor control and had significantly extended survival in two distinct orthotopic DMG models. Notably, the combination resulted in the most extended survival observed, without treatment-related toxicity. This enhanced efficacy is likely mediated by mitochondrial stress induced by ONC206 and apoptotic priming in tumor cells, increasing their susceptibility to immune-mediated killing. However, despite a clear trend observed in our DMG/DIPG models, not all responded equally, underscoring the complexity of DIPG biology and the need for model-specific strategies.

Limitations of this work include the lack of repeated intracranial CAR T cell dosing, which is a primary strategy currently used in patients. As CNS catheter implantation systems have

emerged^{45,46}, future studies will incorporate less aggressive *in vivo* models to provide an opportunity for long term ONC206 dosing and repeated ICV CAR T cell doses. This work will allow future longer-term studies that have the potential to allow for blocks of therapy and other innovative combinatorial strategies. Further, we are yet to incorporate immunocompetent models, though work is currently ongoing to pilot recently developed DIPG syngeneic models and mouse-specific B7-H3 CAR T cells. These models will provide avenues for assessments of potential immune modulation by ONC206 and of potential inhibitory microenvironmental factors that must be addressed for patient therapeutic success. Importantly, our data align with emerging insights from Ziegler and colleagues⁴⁷, who recently demonstrated that the sequence in which combination therapies are delivered can critically influence treatment efficacy in DIPG. This reinforces the rationale for building strategically ordered regimens that both sensitize tumors and support immune function.

Ultimately, this work contributes to a growing, joint international effort to develop rational, mechanism-informed combination approaches that have a higher chance of translational success⁴⁸⁻⁵⁰. Future studies should define the optimal sequence and timing for integrating B7-H3 CAR T cells with ONC206 and exploring its potential in other B7-H3-expressing or immune-evasive tumors.

Conflict of interest

A.T., E.Z.S., J.B.F., M.C.J., and N.A.V. are inventors on issued and pending patents related to CAR T cell therapies. M.C.J. holds equity in and is the Chief Scientific Officer of BrainChild Bio, Inc. M.C.J. holds equity in, is a Board Observer for and serves as a member of the Joint Steering Committee of Umoja Biopharma, Inc. N.A.V. holds equity in and serves as the Scientific Advisory Board Chair for BrainChild Bio, Inc. All other authors declare no competing interests.

Funding

We thank the funding provided by the ChadTough Defeat DIPG Foundation (A.T.), the American-Italian Cancer Foundation (A.T.), the Washington Research Foundation (E.Z.S.), the Invent at Seattle Children's Postdoctoral Scholars Program (E.Z.S.), the Yuvaan Tiwari Foundation (N.A.V.), the DIPG/DMG Research Funding Alliance (N.A.V.), the We Love You Connie

Foundation (N.A.V.), the St. Baldrick's Foundation (N.A.V.), and the National Cancer Institute of the National Institutes of Health (NIH) (R37CA289981; N.A.V.). The content is solely the responsibility of the authors and does not necessarily represent the official views of the NIH. We also thank the generous support from the Avery Huffman DIPG Foundation, Ezra Blue's Flight for Cancer, Live Like a Unicorn, Live Gray's Way, Love for Lucy, the McKenna Claire Foundation, the Pediatric Brain Tumor Research Fund Guild of Seattle Children's, the Team Cozzi Foundation, and Unravel Pediatric Cancer.

Data availability statement

All requests for raw and analyzed data and materials will be promptly reviewed by the Intellectual Property Office of Seattle Children's Research Institute to determine whether the request is subject to any confidentiality or intellectual property restrictions. Raw preclinical data are securely stored at Seattle Children's with indefinite backup. The data supporting the findings of this study are available from the corresponding author upon reasonable request. Any data and materials that can be shared via a Material Transfer Agreement.

Acknowledgements

The authors would like to acknowledge the generosity of all patients and their families. We thank the services provided by Seattle Children's administrative staff, Flow Cytometry Core, and Office of Animal Care, as well as the Experimental Histopathology Shared Resource (RRID:SCR 022606) of the Fred Hutch/University of Washington/Seattle Children's Cancer Consortium (P30 CA015704). We thank Chimerix for providing the drug ONC206, although Oncoceutics, Chimerix, and Jazz Pharmaceuticals did not provide salary support or research funding for any component of this project.

652 **Authorship statement**

653 AT: Design and execution of experiments, supervision, analysis, interpretation of data, writing,
654 and funding acquisition. EZS: Design and execution of experiments, analysis and interpretation
655 of data. RT: Design and execution of experiments, analysis and interpretation of data. LES:
656 Execution of experiments, analysis and interpretation of data. MM: Execution of experiments,
657 analysis and interpretation of data. CP: Execution of experiments, analysis and interpretation of
658 data. KN: Execution of analysis and interpretation of data. AK: Execution of experiments, analysis
659 and interpretation of data. DL: Execution of experiments. SJ: Execution of experiments. AR:
660 Execution of analysis and interpretation of data. JPW: Execution of experiments, analysis and
661 interpretation of data. RR: critical reading of the manuscript. JG: Resources and methodology.
662 CK: Critical reading of the manuscript. ME: Supervision. SP: Supervision. MCJ: Supervision,
663 resources, and critical reading of the manuscript. JBF: Resources, methodology, and critical
664 reading of the manuscript. MDD: Resources and methodology. MCB: Supervision and critical
665 reading of the manuscript. NAV: Design of the study, interpretation of data, supervision, writing,
666 and funding acquisition. All authors read and approved the final manuscript.

667

668

669

References

1. Cooney T, Lane A, Bartels U, et al. Contemporary survival endpoints: an International Diffuse Intrinsic Pontine Glioma Registry study. *Neuro-oncology*. 2017; 19(9):1279-1280.
2. Vitanza NA, Monje M. Diffuse Intrinsic Pontine Glioma: From Diagnosis to Next-Generation Clinical Trials. *Curr Treat Options Neurol*. 2019; 21(8):37.
3. Leitner J, Klauser C, Pickl WF, et al. B7-H3 is a potent inhibitor of human T-cell activation: No evidence for B7-H3 and TREML2 interaction. *Eur J Immunol*. 2009; 39(7):1754-1764.
4. Lei X, Ou Z, Yang Z, et al. A Pan-Histone Deacetylase Inhibitor Enhances the Antitumor Activity of B7-H3-Specific CAR T Cells in Solid Tumors. *Clinical cancer research : an official journal of the American Association for Cancer Research*. 2021; 27(13):3757-3771.
5. Majzner RG, Theruvath JL, Nellan A, et al. CAR T Cells Targeting B7-H3, a Pan-Cancer Antigen, Demonstrate Potent Preclinical Activity Against Pediatric Solid Tumors and Brain Tumors. *Clinical cancer research : an official journal of the American Association for Cancer Research*. 2019; 25(8):2560-2574.
6. Haydar D, Houke H, Chiang J, et al. Cell-surface antigen profiling of pediatric brain tumors: B7-H3 is consistently expressed and can be targeted via local or systemic CAR T-cell delivery. *Neuro-oncology*. 2021; 23(6):999-1011.
7. Vitanza NA, Wilson AL, Huang W, et al. Intraventricular B7-H3 CAR T Cells for Diffuse Intrinsic Pontine Glioma: Preliminary First-in-Human Bioactivity and Safety. *Cancer discovery*. 2023; 13(1):114-131.
8. Vitanza NA, Ronsley R, Choe M, et al. Intracerebroventricular B7-H3-targeting CAR T cells for diffuse intrinsic pontine glioma: a phase 1 trial. *Nat Med*. 2025; 31(3):861-868.
9. Theruvath J, Sotillo E, Mount CW, et al. Locoregionally administered B7-H3-targeted CAR T cells for treatment of atypical teratoid/rhabdoid tumors. *Nat Med*. 2020; 26(5):712-719.
10. Tang M, Chen C, Wang G, et al. Evaluation of B7-H3 Targeted Immunotherapy in a 3D Organoid Model of Craniopharyngioma. *Biomolecules*. 2022; 12(12).
11. Chen C, Wang Y, Zhong K, et al. Frequent B7-H3 overexpression in craniopharyngioma. *Biochem Biophys Res Commun*. 2019; 514(2):379-385.
12. Nehama D, Di Ianni N, Musio S, et al. B7-H3-redirected chimeric antigen receptor T cells target glioblastoma and neurospheres. *EBioMedicine*. 2019; 47:33-43.
13. Digregorio M, Coppieters N, Lombard A, Lumapat PN, Scholtes F, Rogister B. The expression of B7-H3 isoforms in newly diagnosed glioblastoma and recurrence and their functional role. *Acta Neuropathol Commun*. 2021; 9(1):59.
14. Wang Z, Wang Z, Zhang C, et al. Genetic and clinical characterization of B7-H3 (CD276) expression and epigenetic regulation in diffuse brain glioma. *Cancer Sci*. 2018; 109(9):2697-2705.
15. Marques RF, Moreno DA, da Silva L, et al. Digital expression profile of immune checkpoint genes in medulloblastomas identifies CD24 and CD276 as putative immunotherapy targets. *Front Immunol*. 2023; 14:1062856.
16. Li S, Poolen GC, van Vliet LC, et al. Pediatric medulloblastoma express immune checkpoint B7-H3. *Clin Transl Oncol*. 2022; 24(6):1204-1208.
17. Deng J, Ma M, Wang D, et al. Expression and Clinical Significance of Immune Checkpoint Regulator B7-H3 (CD276) in Human Meningioma. *World Neurosurg*. 2020; 135:e12-e18.
18. Proctor DT, Patel Z, Lama S, Resch L, van Marle G, Sutherland GR. Identification of PD-L2, B7-H3 and CTLA-4 immune checkpoint proteins in genetic subtypes of meningioma. *Oncoimmunology*. 2019; 8(1):e1512943.
19. Castriconi R, Dondero A, Augugliaro R, et al. Identification of 4Ig-B7-H3 as a neuroblastoma-associated molecule that exerts a protective role from an NK cell-mediated lysis. *Proc Natl Acad Sci U S A*. 2004; 101(34):12640-12645.

20. Timpanaro A, Piccand C, Uldry AC, et al. Surfaceome Profiling of Cell Lines and Patient-Derived Xenografts Confirm FGFR4, NCAM1, CD276, and Highlight AGRL2, JAM3, and L1CAM as Surface Targets for Rhabdomyosarcoma. *Int J Mol Sci.* 2023; 24(3).
21. Lavoie RR, Gargollo PC, Ahmed ME, et al. Surfaceome Profiling of Rhabdomyosarcoma Reveals B7-H3 as a Mediator of Immune Evasion. *Cancers (Basel).* 2021; 13(18).
22. Prabhu VV, Allen JE, Dicker DT, El-Deiry WS. Small-Molecule ONC201/TIC10 Targets Chemotherapy-Resistant Colorectal Cancer Stem-like Cells in an Akt/Foxo3a/TRAIL-Dependent Manner. *Cancer Res.* 2015; 75(7):1423-1432.
23. Jackson ER, Persson ML, Fish CJ, et al. A review of current therapeutics targeting the mitochondrial protease ClpP in diffuse midline glioma, H3 K27-altered. *Neuro Oncol.* 2024; 26(Supplement_2):S136-S154.
24. Allen JE, Kline CL, Prabhu VV, et al. Discovery and clinical introduction of first-in-class imipridone ONC201. *Oncotarget.* 2016; 7(45):74380-74392.
25. Ishizawa J, Zarabi SF, Davis RE, et al. Mitochondrial ClpP-Mediated Proteolysis Induces Selective Cancer Cell Lethality. *Cancer Cell.* 2019; 35(5):721-737 e729.
26. Graves PR, Aponte-Collazo LJ, Fennell EMJ, et al. Mitochondrial Protease ClpP is a Target for the Anticancer Compounds ONC201 and Related Analogues. *ACS Chem Biol.* 2019; 14(5):1020-1029.
27. Przystal JM, Cianciolo Cosentino C, Yadavilli S, et al. Imipridones affect tumor bioenergetics and promote cell lineage differentiation in diffuse midline gliomas. *Neuro Oncol.* 2022; 24(9):1438-1451.
28. Tucker K, Yin Y, Staley SA, et al. ONC206 has anti-tumorigenic effects in human ovarian cancer cells and in a transgenic mouse model of high-grade serous ovarian cancer. *Am J Cancer Res.* 2022; 12(2):521-536.
29. Biery MC, Noll A, Myers C, et al. A Protocol for the Generation of Treatment-naïve Biopsy-derived Diffuse Intrinsic Pontine Glioma and Diffuse Midline Glioma Models. *J Exp Neurol.* 2020; 1(4):158-167.
30. Vitanza NA, Biery MC, Myers C, et al. Optimal therapeutic targeting by HDAC inhibition in biopsy-derived treatment-naïve diffuse midline glioma models. *Neuro-oncology.* 2021; 23(3):376-386.
31. Maachani UB, Tosi U, Pisapia DJ, et al. B7-H3 as a Prognostic Biomarker and Therapeutic Target in Pediatric central nervous system Tumors. *Transl Oncol.* 2020; 13(2):365-371.
32. Zhou Z, Luther N, Ibrahim GM, et al. B7-H3, a potential therapeutic target, is expressed in diffuse intrinsic pontine glioma. *Journal of neuro-oncology.* 2013; 111(3):257-264.
33. Noll A, Myers C, Biery MC, et al. Therapeutic HDAC inhibition in hypermutant diffuse intrinsic pontine glioma. *Neoplasia.* 2023; 43:100921.
34. Lin GL, Wilson KM, Ceribelli M, et al. Therapeutic strategies for diffuse midline glioma from high-throughput combination drug screening. *Sci Transl Med.* 2019; 11(519).
35. Jane EP, Reslink MC, Gatesman TA, et al. Targeting mitochondrial energetics reverses panobinostat- and marizomib-induced resistance in pediatric and adult high-grade gliomas. *Mol Oncol.* 2023; 17(9):1821-1843.
36. Batsios G, Taglang C, Udutha S, et al. Lactylation fuels nucleotide biosynthesis and facilitates deuterium metabolic imaging of tumor proliferation in H3K27M-mutant gliomas. *bioRxiv.* 2025.
37. Mueller T, Laternser S, Guerreiro Stucklin AS, et al. Real-time drug testing of paediatric diffuse midline glioma to support clinical decision making: The Zurich DIPG/DMG centre experience. *Eur J Cancer.* 2023; 178:171-179.
38. Jackson ER, Duchatel RJ, Staudt DE, et al. ONC201 in Combination with Paxalisib for the Treatment of H3K27-Altered Diffuse Midline Glioma. *Cancer Res.* 2023:OF1-OF17.
39. Duchatel RJ, Jackson ER, Parackal SG, et al. PI3K/mTOR is a therapeutically targetable genetic dependency in diffuse intrinsic pontine glioma. *J Clin Invest.* 2024; 134(6).

- 770 **40.** Mueller T, Yadavilli S, Laternser S, et al. HGG-24. PRECLINICAL EFFICACY OF THE
771 BRAIN PENETRANT CYCLIN-DEPENDENT KINASE INHIBITOR ZOTIRACICLIB IN
772 PEDIATRIC DIFFUSE MIDLINE GLIOMAS. (1522-8517 (Print)).
- 773 **41.** Duchatel RJ, Jackson ER, Parackal SG, et al. PI3K/mTOR is a therapeutically targetable
774 genetic dependency in diffuse intrinsic pontine glioma. *The Journal of clinical investigation*.
775 2024.
- 776 **42.** Staley A, Tucker K, Yin Y, et al. Highly potent dopamine receptor D2 antagonist ONC206
777 demonstrates anti-tumorigenic activity in endometrial cancer. *Am J Cancer Res*. 2021;
778 11(11):5374-5387.
- 779 **43.** Monzer A, Ghamlouche F, Wakimian K, et al. ONC206, an imipridone derivative,
780 demonstrates anti-colorectal cancer activity against stem/progenitor cells in 3D cell
781 cultures and in patient-derived organoids. *Pharmacol Rep*. 2024.
- 782 **44.** Jackson ER, Duchatel RJ, Staudt DE, et al. ONC201 in combination with paxalisib for the
783 treatment of H3K27-altered diffuse midline glioma. *Cancer Res*. 2023; 83(14):2421-2437.
- 784 **45.** Foster JB, Madsen PJ, Harvey K, et al. Transient mRNA CAR T cells targeting GD2
785 provide dose-adjusted efficacy against diffuse midline glioma and high grade glioma
786 models. *Neuro-oncology*. 2025.
- 787 **46.** Harvey K, Madsen PJ, Smith T, et al. Intracranial Cannula Implantation for Serial
788 Locoregional Chimeric Antigen Receptor (CAR) T Cell Infusions in Mice. *J Vis Exp*.
789 2023(192).
- 790 **47.** Khan A, Upton D, Gopalakrishnan A, Chen Y, Tsoli M, Ziegler DS. DIPG-46. TOTAL
791 THERAPY FOR DIFFUSE MIDLINE GLIOMAS: A SEQUENTIAL, INTENSIVE, MULTI-
792 AGENT COMBINATION PLATFORM IS A POTENT TREATMENT STRATEGY. *Neuro-*
793 *Oncology*. 2024; 26(Supplement_4):0-0.
- 794 **48.** Ehteda A, Simon S, Franshaw L, et al. Dual targeting of the epigenome via FACT complex
795 and histone deacetylase is a potent treatment strategy for DIPG. (2211-1247 (Electronic)).
- 796 **49.** Duchatel RJ, Jackson ER, Parackal SG, et al. PI3K/mTOR is a therapeutically targetable
797 genetic dependency in diffuse intrinsic pontine glioma. LID - 10.1172/JCI170329 [doi] LID
798 - e170329. (1558-8238 (Electronic)).
- 799 **50.** Persson ML, Douglas AM, Alvaro F, et al. The intrinsic and microenvironmental features
800 of diffuse midline glioma: Implications for the development of effective immunotherapeutic
801 treatment strategies. (1523-5866 (Electronic)).
- 802 **51.** Timpanaro A, Piccand C, Dzhumashev D, et al. CD276-CAR T cells and Dual-CAR T cells
803 targeting CD276/FGFR4 promote rhabdomyosarcoma clearance in orthotopic mouse
804 models. *J Exp Clin Cancer Res*. 2023; 42(1):293.
- 805 **52.** Chen S, Zhou Y, Chen Y, Gu J. fastp: an ultra-fast all-in-one FASTQ preprocessor.
806 *Bioinformatics*. 2018; 34(17):i884-i890.
- 807 **53.** Chen S. Ultrafast one-pass FASTQ data preprocessing, quality control, and deduplication
808 using fastp. *Imeta*. 2023; 2(2):e107.
- 809 **54.** Harrison PA-O, Amode MR, Austine-Orimoloye O, et al. Ensembl 2024. (1362-4962
810 (Electronic)).
- 811 **55.** Bray NL, Pimentel H, Melsted PA-O, Pachter L. Near-optimal probabilistic RNA-seq
812 quantification. (1546-1696 (Electronic)).
- 813 **56.** Ewels P, Magnusson M, Lundin S, Käller M. MultiQC: summarize analysis results for
814 multiple tools and samples in a single report. (1367-4811 (Electronic)).
- 815 **57.** Soneson C, Love MI, Robinson MD. Differential analyses for RNA-seq: transcript-level
816 estimates improve gene-level inferences. (2046-1402 (Print)).
- 817 **58.** Chen Y, Lun AT, Smyth GK. From reads to genes to pathways: differential expression
818 analysis of RNA-Seq experiments using Rsubread and the edgeR quasi-likelihood
819 pipeline. (2046-1402 (Print)).

59. McCarthy DJ, Chen Y, Smyth GK. Differential expression analysis of multifactor RNA-Seq experiments with respect to biological variation. (1362-4962 (Electronic)).
60. Robinson MD, McCarthy DJ, Smyth GK. edgeR: a Bioconductor package for differential expression analysis of digital gene expression data. (1367-4811 (Electronic)).
61. Ritchie ME, Phipson B, Wu D, et al. limma powers differential expression analyses for RNA-seq and microarray studies. (1362-4962 (Electronic)).

862 Table 1. Material and methods list.

ITEM	COMPANY	CATALOG NUMBERS
Cell culture		
NeuroCult™ NS-A Proliferation Kit (Human)	Stemcell Technologies	5751
RPMI-1640	Gibco	21870076
DMEM	Gibco	119600044
Fetal Bovine Serum (FBS)	Gibco	A5670701
Laminin	Trevigen	3446-005-01
Rat tail collagen type-I	Millipore Sigma	C3867 1VL
EGF	PeproTech	AF-100-15
FGF	PeproTech	AF-100-18B
GlutaMax	ThermoFisher	35050061
Cryostor CS10	StemCell Technologies	100-1061
P10 dishes	Greiner Bio-One CELLSTAR	633181
T75 flasks	Corning	430641U
T150 flasks	Corning	430825U
96-well white flat bottom plates	Greiner Bio-One CELLSTAR	07-000-138
96-well black flat bottom plates	Fisher Scientific	08-772-225
24-well transparent flat bottom plates	Greiner bio-One	662160
D-Luciferin substrate	Revvity	122799-5
EasySep™ Human T cell isolation kit	StemCell Technologies	17951
Recombinant human IL 7	BioLegend	581904
Recombinant human IL 15	BioLegend	570304
Plasmids		
psPAX2	Addgene	12260
pVSV-G	Addgene	8454
Caspase assays		
Incucyte Caspase 3/7 assay	Sartorius	4440
Compounds		
Carboplatin (50 mg)	MedChem	HY-17393
ONC206	Chemspec API	031000
Etoposide	MedChem	HY-13629
Everolimus (50 mg)	MedChem	HY-10218
Marizomib (100 ug)	Sigma Aldrich	SML1916-100UG
Pacritinib	MedChem	HY-16379
Paxalisib	MedChem	HY-19962
Vincristine sulfate (10 mg)	SelleckChem	S1241
Zotiraciclib	MedChem	HY-15163
Seahorse Technology		
Seahorse Cell Mito-Stress kit	Agilent Technologies	103015-100
XF RPMI medium, pH 7.4	Agilent Technologies	103576-100
XF 1.0M Glucose	Agilent Technologies	103577-100
XF 100 mM Pyruvate	Agilent Technologies	103578-100
XF 200 mM Glutamine	Agilent Technologies	103579-100
CellTiter-Glo™ 2.0 Assay	Promega	PRG9243
Enzyme-linked immunosorbent assay		
IL-2 DuoSet ELISA development system	R&D Systems	DY202
TNF-α DuoSet ELISA development system	R&D Systems	DY202-05
IFN-γ DuoSet ELISA development system	R&D Systems	DY285B
RNA extration		
RNeasy Plus Mini Kit	Qiagen	74134
Primary Antibodies		
Brilliant Violet 421™ anti-human CD62L	BioLegend	304828

Brilliant Violet 510™ anti-human CD3	BioLegend	317332
Brilliant Violet 605™ anti-human CCR7	BioLegend	353224
FITC anti-human CD4	BioLegend	300530
PECy7 anti-human CD95	BioLegend	305622
PE anti-human CD45RA	BioLegend	304108
APC anti-human CCR5	BioLegend	359122
Alexa Fluor® 700 anti-human CD8a	BioLegend	301028
PE anti-human B7-H3	BioLegend	351004
FITC Annexin V Apoptosis Detection Kit	BioLegend	640922

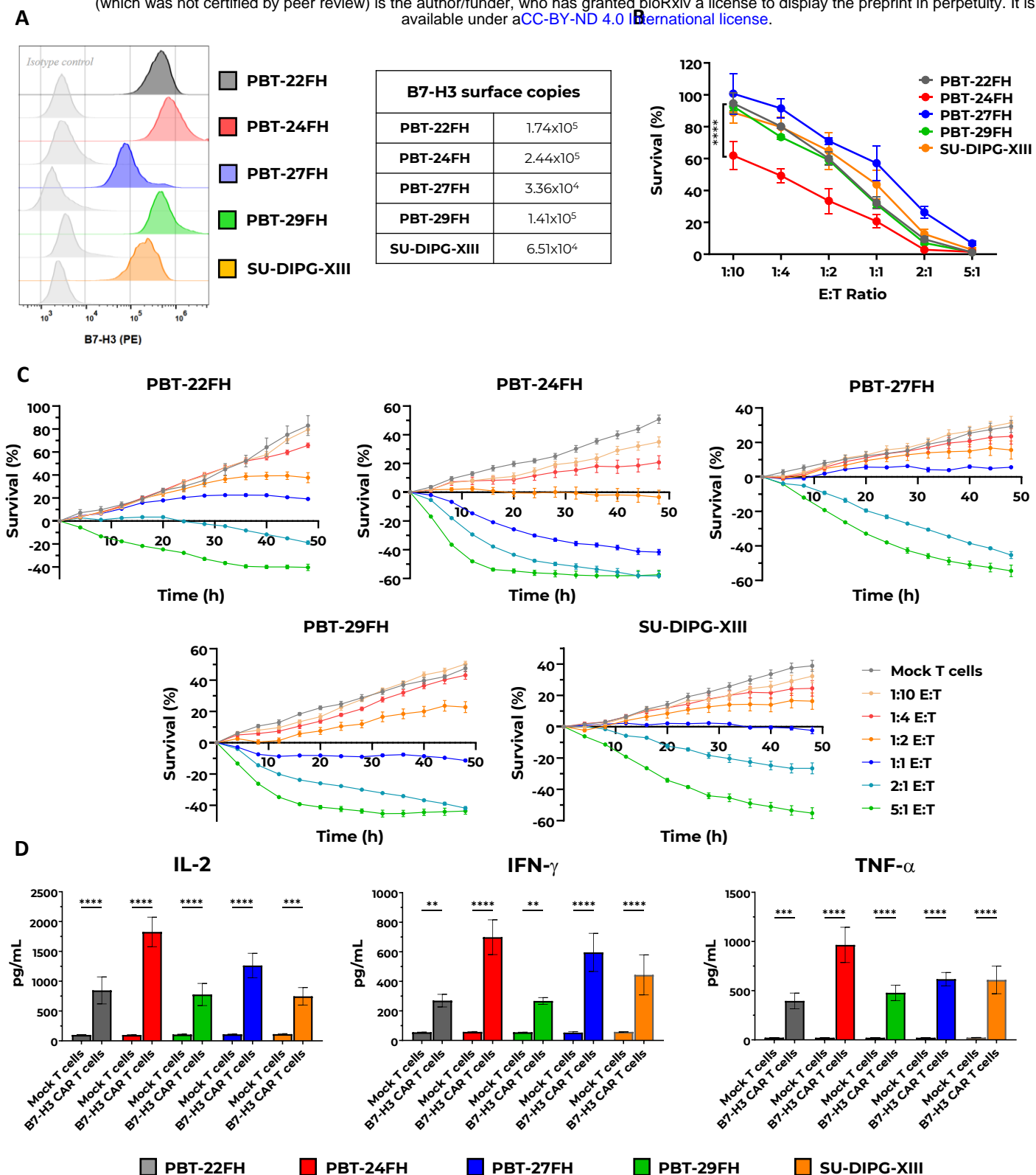


Figure 1 - B7-H3 expression on DIPG models and efficacy of B7-H3 CAR T cells. **A.** B7-H3 expression was assessed in PBT-22FH, PBT-24FH, PBT-27FH, PBT-29FH, and SU-DIPG-XIII models using flow cytometry. High levels of B7-H3 were uniformly detected across all models with a PE-conjugated anti-B7-H3 antibody. Surface copy numbers of B7-H3 molecules were quantified with BD Quantibrite beads. **B.** B7-H3 CAR T cell killing capacity was determined after co-incubation of CAR T cells with fLuc⁺ iRFP720⁺ DIPG cells at different Effector-to-Target (E:T) ratios. Tumor cell survival (%) was evaluated at a single 48-hour time point using luciferase assays. Significantly higher killing was observed against PBT-24FH, compared to the other models. $P < 0.001$ ($n = 3$ donors). **C.** Live-imaging experiments assessed the effectiveness of low-doses of B7-H3 CAR T cells ($n = 3$ donors) against DIPG models at multiple time-points, serving as a preliminary step to explore enhanced combinatorial killing with ONC206. These results, normalized to the respective measurements at $t = 0$ h, report the most representative donor. **D.** Cytokine release of IL-2, IFN- γ , and TNF- α from B7-H3 CAR T cells was assessed via ELISA after 24h co-incubation with DIPG cells ($n = 3$ donors). ns = not significant; $p < 0.05$; $p < 0.01$; $p < 0.001$.

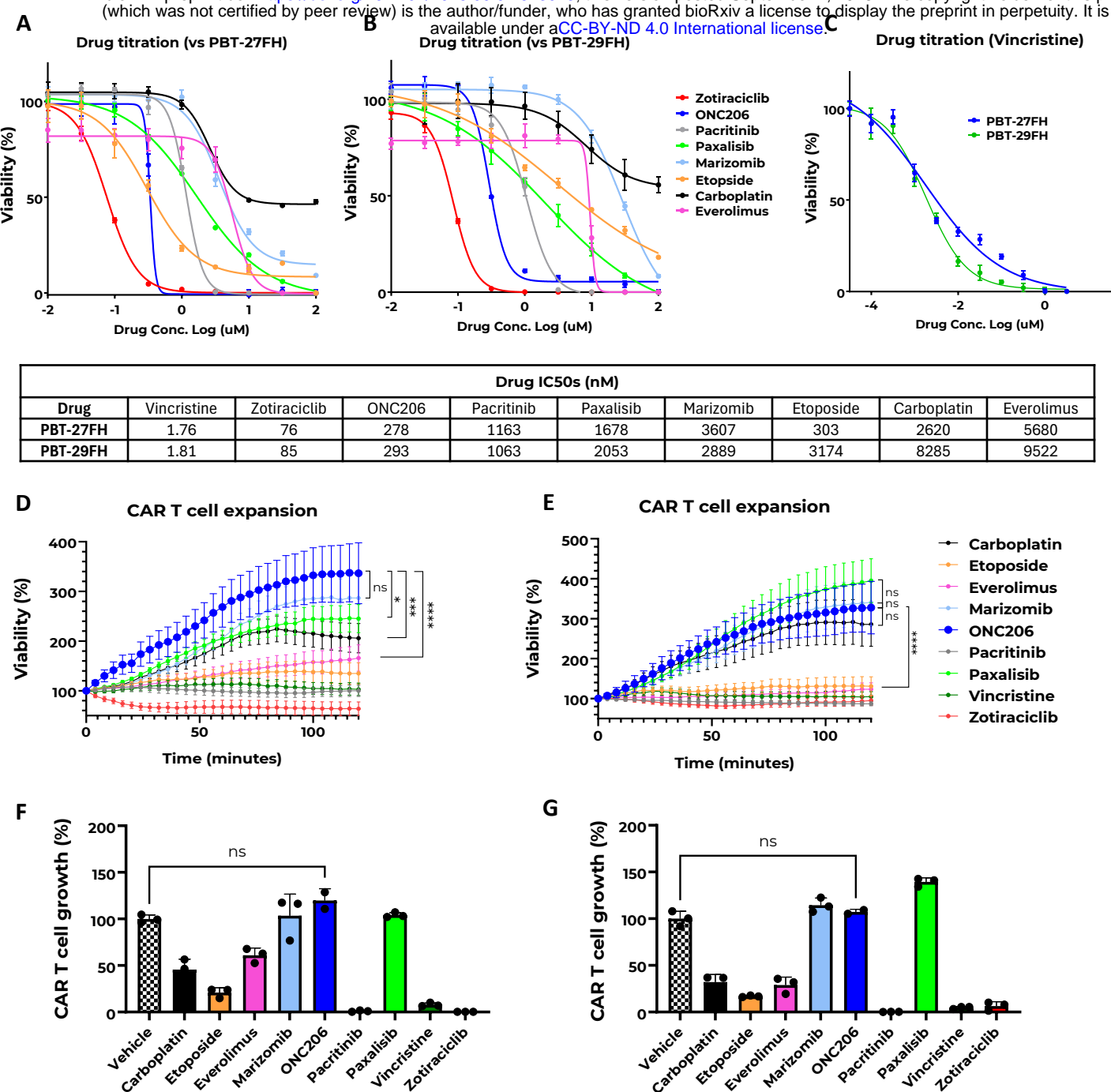


Figure 2. ONC206 selection from a 9-drug panel and its impact on B7-H3 CAR T cell viability and expansion. A-B. Dose-response curves of PBT-27FH (A) and PBT-29FH (B) DIPG cell lines following 120-hour treatment with a panel of drugs: Carboplatin, Etoposide, Everolimus, Marizomib, ONC206, Pacritinib, Paxalisib, Vincristine, and Zotiraciclib. IC₅₀ values were calculated for each condition. **C.** Vincristine titration curve shown using a log concentration range of -4.5 to 0.5 due to its high potency. IC₅₀ values were comparable between PBT-27FH and PBT-29FH cells. A summary of IC₅₀ values is provided in the accompanying table. **D-E.** B7-H3 CAR T cell expansion in co-culture with PBT-27FH (D) or PBT-29FH (E) cells over 120 hours. CAR T cells were co-cultured at an effector-to-target (E:T) ratio of 5:1 for 24 hours, followed by treatment with the respective drugs at their respective IC₅₀ concentrations. ONC206, Marizomib, Paxalisib, and Carboplatin did not impair CAR T cell expansion, whereas Etoposide, Everolimus, Pacritinib, Vincristine, and Zotiraciclib significantly inhibited CAR T cell proliferation. **F-G.** Quantification of CAR T cell growth at 120 hours post-drug exposure in PBT-27FH (F) and PBT-29FH (G) co-cultures, normalized to vehicle control. ns = not significant; $p < 0.05$; $p < 0.01$; $p < 0.001$.

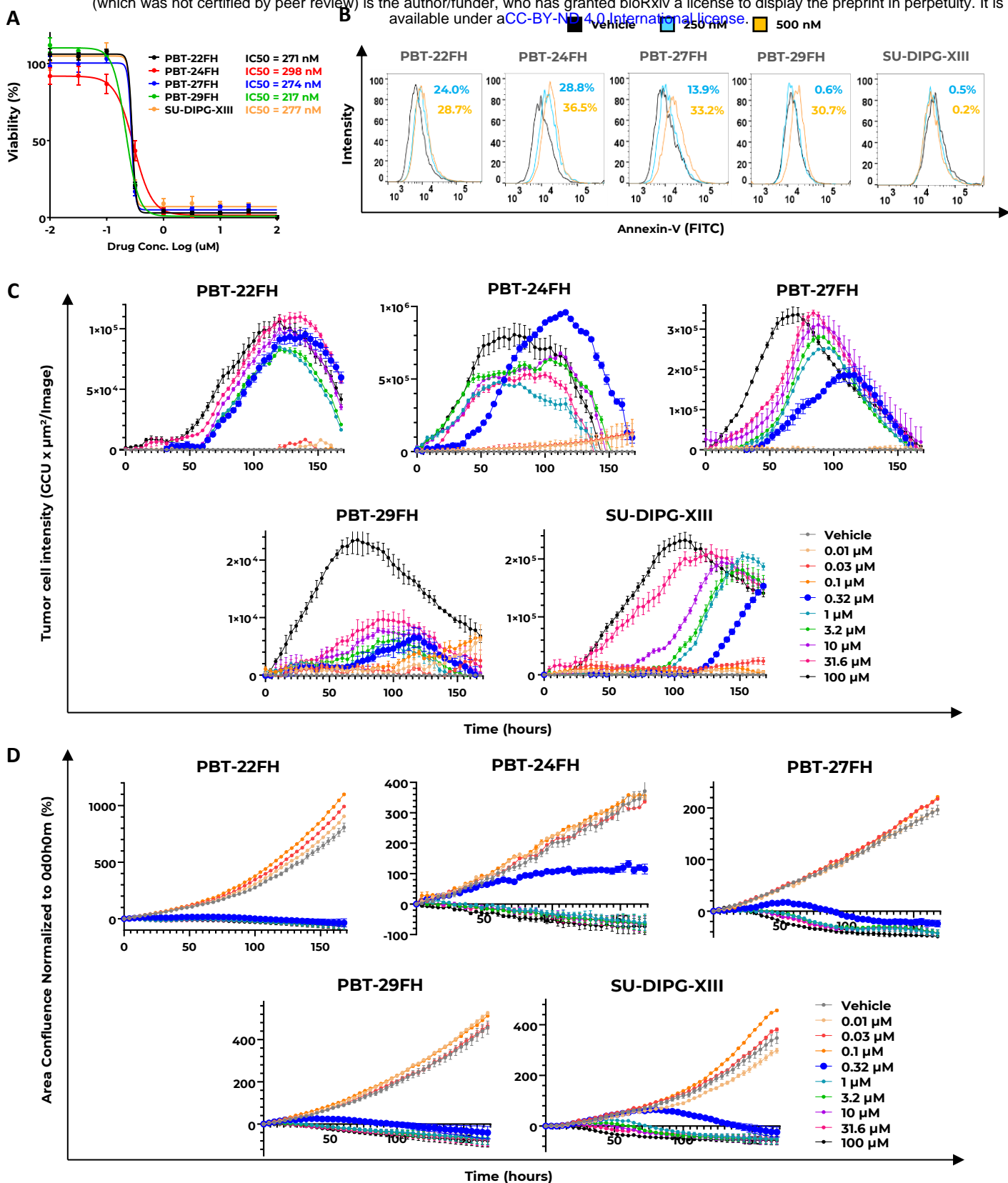


Figure 3 - ONC206 cytotoxicity and apoptosis induction in DIPG models. **A.** ONC206 IC₅₀ values were determined for PBT-22FH, PBT-24FH, PBT-27FH, PBT-29FH, and SU-DIPG-XIII cells. Tumor cells were incubated with varying concentrations of ONC206, and cell survival was assessed using cytotoxicity assays after 120 hours. Dose-response curves indicate consistent IC₅₀ values ranging from 217 to 298 nM across DIPG cell lines. **B.** Early apoptosis was evaluated by flow cytometry. DIPG cells were treated with ONC206 at 250 nM (blue) and 500 nM (orange) for 48 hours, and Annexin-V levels were quantified using CytoFlex. **C.** Apoptosis induction by ONC206 was assessed in 7-day live-imaging assays by monitoring Caspase-3/-7 activation using a green fluorescence dye. An apoptotic peak near IC₅₀ concentrations was observed at 120 hours in all models except SU-DIPG-XIII, which showed greater tolerance to apoptosis. **D.** Live-imaging experiments confirmed the efficacy of ONC206 at concentrations $\geq 0.32 \mu\text{M}$. PBT-24FH and SU-DIPG-XIII exhibited partial resilience at 0.32 μM . All experiments were performed in biological triplicates ($n = 3$), with representative data shown.

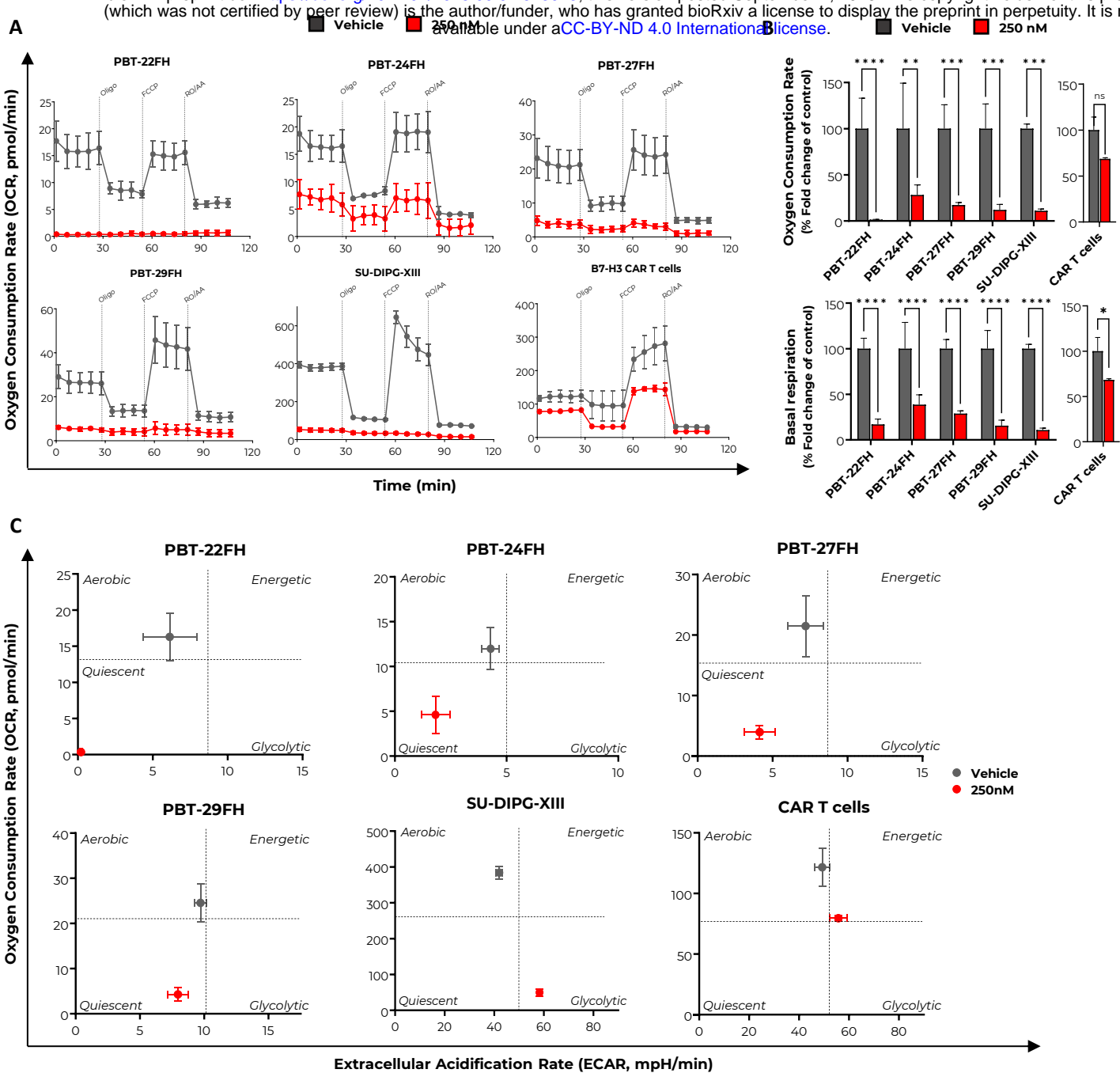


Figure 4 – Respiratory response to ONC206 treatment in DIPG models and CAR T cells. PBT-22FH, PBT-24FH, PBT-27FH, PBT-29FH, SU-DIPG-XIII tumor cells and B7-H3 CAR T cells were treated with ONC206 at 250 nM (red) for 48 hours, and metabolic parameters were evaluated using Agilent Seahorse XF Technology. **A.** Oxygen consumption rate (OCR) profiles were measured over 100 minutes following sequential addition of oligomycin, FCCP, and rotenone/antimycin. Compared to the vehicle (gray), the IC50 dose (250 nM) impaired OCR in DIPG cells, while CAR T cells exhibited only a limited reduction. Fold-change bar charts for metabolic parameters, such as OCR and basal respiration, were quantified for all the investigated DIPG cells and CAR T cells, highlighting the significant resilience of CAR T cells at IC50 doses. **B.** Bioenergetics plots illustrate a metabolic shift in all the investigated DIPG models toward glycolytic or quiescent states under ONC206 treatment. In contrast, CAR T cells maintained an energetic phenotype, showing better tolerance to mitochondrial stress. All experiments were performed in triplicates (n = 3), with the most representative data shown.

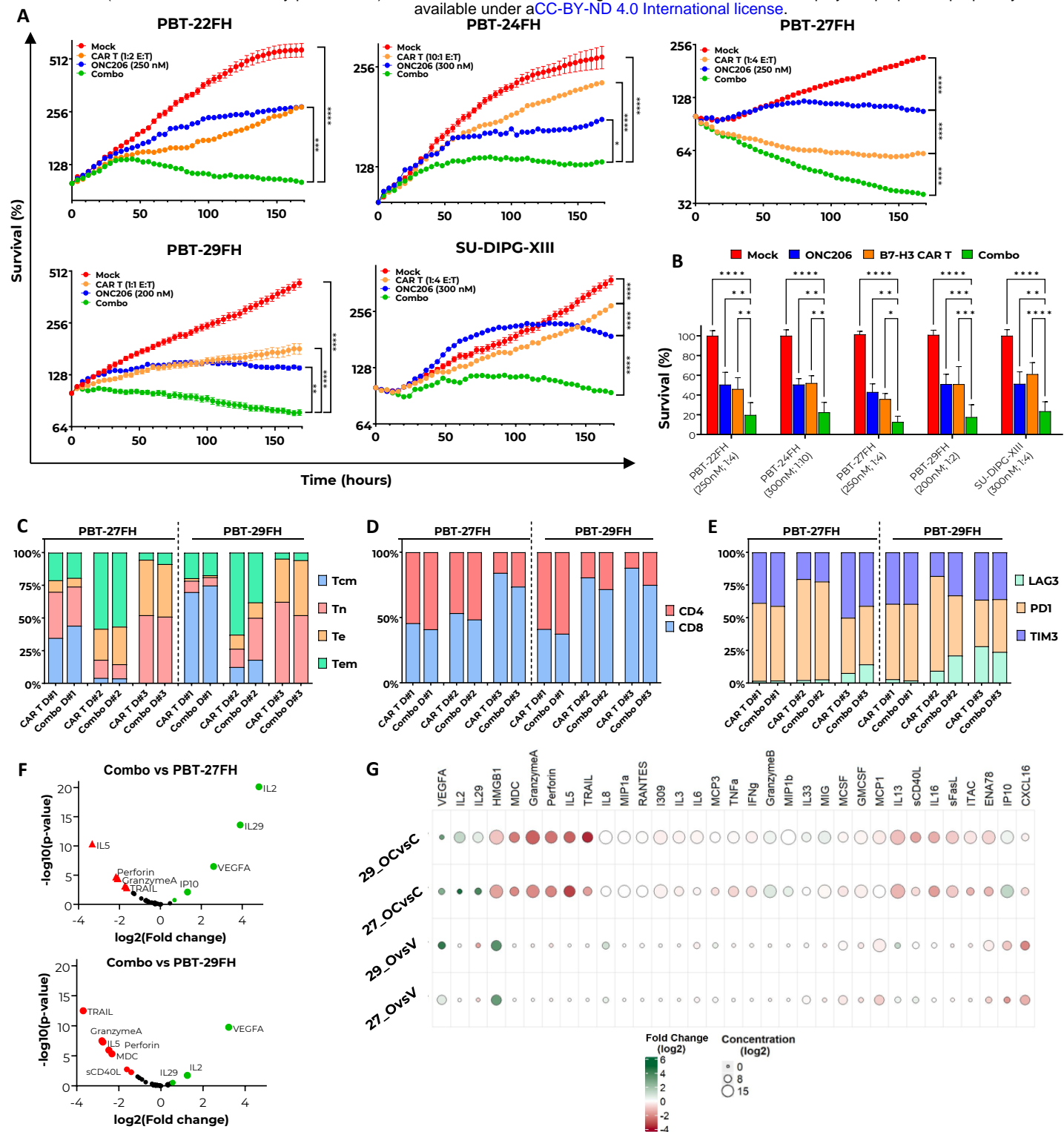


Figure 5 – Low doses of ONC206 improve killing and preserve functional properties of B7-H3 CAR T cells. DIPG cell killing was evaluated under combinatorial conditions of ONC206 and B7-H3 CAR T cells, while variation of CAR T cell properties was assessed via flow cytometry and multiplex immunoassays after 5 days of ONC206 treatment. **A.** Incucyte technology was used to monitor DIPG cell survival for seven days. Combinatorial benefit (green) is compared to single treatments of low E:T ratios of CAR T cells (orange) and IC50 doses of ONC206 (blue). Mock T cells were used as negative control (red). **B.** Bioluminescence assays confirmed significant combinatorial benefit (green) after 120 hours of co-culture. **C–E.** CAR T cell phenotype, CD4/CD8 ratios, and CAR T cell exhaustion were evaluated by flow cytometry revealing non-significant changes between treated- and untreated-CAR T cells. D#1, #2, #3 represent the three T cell donors used. **F.** P-value vs fold-change charts highlight significantly increased levels of IL-2, IL-29, IP10, and VEGF-A, and decreased levels of TRAIL, Granzyme-A, IL-5, and perforins in PBT-27FH and PBT-29FH post-5-day treatment with ONC206 (250 nM). **G.** Bubble heatmap of 33 cytokines show contrasts of interest (“Combo vs CAR T alone” and “ONC206 vs vehicle”) for each cell line. Each bubble color indicates the log2 FC derived from the linear mixed-effects model (green = positive FC; red = negative FC). The bubble size corresponds to the average log2 cytokine concentration for each comparison’s control (no drug). All pairwise contrasts were FDR-adjusted.

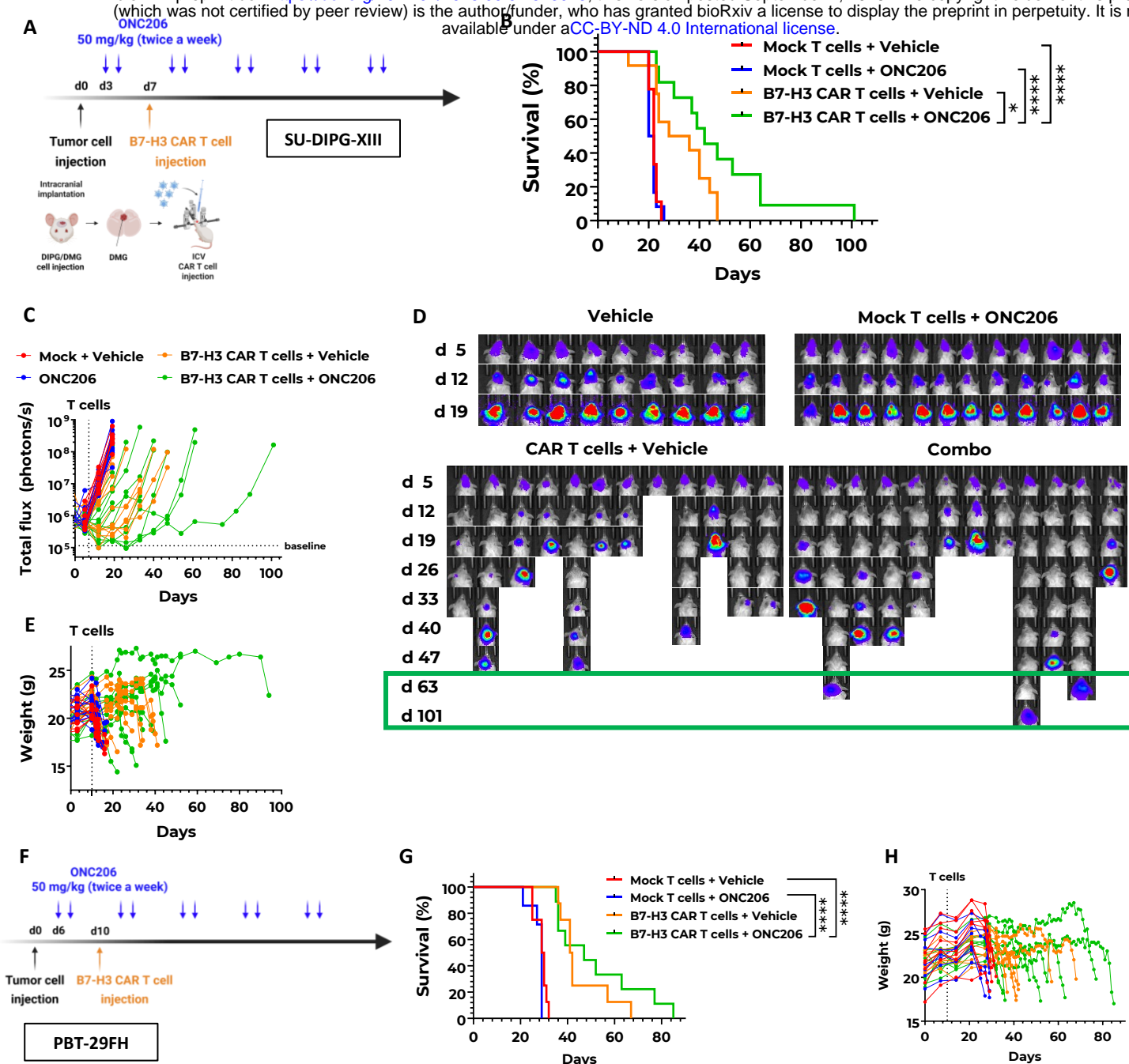


Figure 6 - ONC206/B7-H3 CAR T cell combinatorial treatment showed significant extended survival in DIPG models. (A) Schematic representation of the experimental timeline for B7-H3 CAR T cell treatment in combination with ONC206 against the SU-DIPG-XIII model. Tumor-bearing mice received ONC206 (50 mg/kg) at the indicated time points following T cell injection. 1 million mock T cells/B7-H3 CAR T cells were ICV injected at day 7. **(B)** Kaplan-Meier survival curve comparing the different treated groups shows a subset of mice with long-term tumor control able to delay survival up to 94 days. **(C)** Tumor burden progression, measured by bioluminescence imaging (total flux), showing improved tumor control in the CAR T cell + ONC206 combination group. **(D)** Representative bioluminescence images of tumor burden over time for each treatment group. The CAR T cell + ONC206 combination resulted in the most effective tumor suppression. **(E)** Weight progression over time across treatment groups. No significant weight loss was observed, indicating treatment tolerance. **(F)** Schematic representation of the experimental timeline for B7-H3 CAR T cells treatment in combination with ONC206 against PBT-29FH model. **(G)** Kaplan-Meier survival curve shows extended survival up to 75 days in the combinatorial group compared to the B7-H3 CAR T cell treatment. Significant difference was observed with ONC206 monotherapy and mock group T cells. **(H)** Weight progression over time across treatment groups. (**** $p < 0.0001$, * $p < 0.05$, log-rank test).